2007

Synthesis and kinetic analysis of tendamistat-based a-amylase inhibitors

Allison Rogalski

Synthesis and kinetic analysis of tendamistat-based a-amylase inhibitors

Abstract

α-Amylase is an enzyme that breaks down polysaccharides into their glucose subunits. It is one of the enzymes important in controlling blood sugar levels in the body. Inhibiting α-amylase could be a beneficial treatment for insulin-dependent diabetes mellitus, obesity, and hyperlipaemia. Naturally occurring Tendamistat has been found with such inhibitory affects, but there are drawbacks to this molecule and a small variation was synthesized. Several variations of the parent were tested in this research, exchanging Tyr15 for other residues to test for how a pKa change affects the inhibitory property. The peptide sequences were synthesized, cleaved, and purified through High Performance Liquid Chromatography before conducting three assays on each that varied in the concentration of inhibitor used. The rates of the reactions were then analyzed using Michealis-Menten and Lineweaver-Burk plots to conclude an average Ki value. In general, as the pKa value for the modification to the parent compound increased, the Ki values also increased, suggesting an importance of hydrogen bonding between the inhibitor and the enzyme.

Degree Type

Open Access Senior Honors Thesis

Department

Chemistry

First Advisor

Dr. Deborah Heyl-Clegg

Second Advisor

Dr. Heather Holmes

Keywords

Amylases Inhibitors, Diabetes Research

SYNTHESIS AND KINETIC ANAYLSIS OF TENDAMISTAT-BASED α-AMYLASE INHIBITORS

By

Allison Rogalski

A Senior Thesis Submitted to the

Eastern Michigan University

Honors College

in Partial Fulfillment of the Requirements for Graduation

with Honors in Chemistry

Approved at Ypsilanti, Michigan, on this date April 20, 2007

_____

Dr. Deborah Heyl-Clegg, Supervising Instructor

_____

Dr. Heather Holmes, Honors Advisor

_____

Dr. Maria Milletti, Department Head

_____

Dr. James Knapp, Honors Director

Table of Contents

Abstract

α-Amylase is an enzyme that breaks down polysaccharides into their glucose subunits. It is one of the enzymes important in controlling blood sugar levels in the body. Inhibiting α-amylase could be a beneficial treatment for insulin-dependent diabetes mellitus, obesity, and hyperlipaemia. Naturally occurring Tendamistat has been found with such inhibitory affects, but there are drawbacks to this molecule and a small variation was synthesized. Several variations of the parent were tested in this research, exchanging Tyr^{15} for other residues to test for how a pKa change affects the inhibitory property. The peptide sequences were synthesized, cleaved, and purified through High Performance Liquid Chromatography before conducting three assays on each that varied in the concentration of inhibitor used. The rates of the reactions were then analyzed using Michealis-Menten and Lineweaver-Burk plots to conclude an average K_i value. In general, as the pKa value for the modification to the parent compound increased, the K_i values also increased, suggesting an importance of hydrogen bonding between the inhibitor and the enzyme.

Introduction

The purpose of this project is to develop a peptide α-amylase inhibitor, which would be beneficial to those suffering from insulin-dependent diabetes mellitus (IDDM), obesity, and hyperlipaemia. α-Amylase is used in the body to hydrolyze the α–D-(1-4) glycosidic bonds in starch, glycogen, amylase, amylopectin, and other polysaccharides into glucose molecules to control blood sugar levels (Cox and Nelson, 2005). α-Amylase is present in saliva and the pancreatic juices. It plays a central role in carbohydrate metabolism and has become one of the most used enzymes in modern biotechnology (Vihinen and Mantsala, 1989). However, in those suffering from IDDM, obesity, or hyperlipaemia, α-amylase can be harmful, so an inhibitor that would prevent α-amylase from performing would be beneficial.

α-Amylase is composed of three domains, 498 amino acids, and its structure can be found in Figure 1. The first of these domains is the central N-terminal domain A, which is comprised of a $(\beta/\alpha)_8$-barrel (Machius et al., 1996). This region serves as a scaffold on which the other domains rest (Machius et al., 1996). The second domain is the B domain, which is a complex loop structure (Machius et al., 1996). The last domain C, which contains a Greek key motif, is the location of the functional sites including the active site and the calcium binding site (Machius et al., 1996).

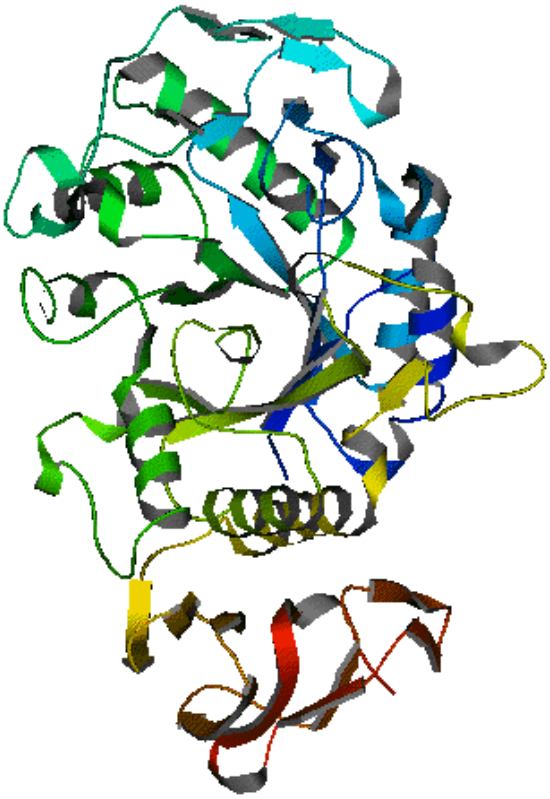

Figure 1. Three-Dimensional Model of the Structure of α-Amylase. ("Alpha Amylase")

Finding an inhibitor to be used therapeutically to solve the problems of IDDM, obesity, and hyperlipaemia would be quite beneficial. It is a problem that has been explored by other researchers. Three types of α-amylase inhibitors have been found: higher plant proteins, microbial N-containing carbohydrates, and microbial peptides (Lee et al., 2002). Lee et al. (2002) has explored the common bean (*Phaseolus vulgaris*) which contains α-amylase inhibitors that exhibit inhibitory activity with some mammalian and insect α-amylases.

Kinetic experiments have been carried out on α-amylase using oligosaccharides. These experiments suggest the existence of a five sugar binding subsite in the active site of porcine pancreatic α-amylase (Machius et al., 1996). This collection of oligosaccharide inhibitors is derived from the trestatin family of *Streptomyces* and

includes acarviosine, an N-linked pseudo-disaccharide and a range in the number of glucose molecules (Machius et al., 1996). Porcine pancreatic α-amylase rearranges the cleavage products of these oligosaccharides, which in turn turns hydrolyzable compounds like the substrate into a non-hydrolyzable compound, resulting in inhibition (Machius et al., 1996). Other oligosaccharides are being researched using non-hexose rings and nonhydrolyzable bonds (Machius et al., 1996).

Proteinaceous inhibitors have also been explored. These include Paim, Haim, Z-2685, T-76, AI-409, and Tendamistat (Machius et al., 1996). All of these inhibitors contain similar amino acid sequences in binding to α-amylase and are all derived from the genus *Streptomyces*. Paim is an animal α-amylase inhibitor derived from *Streptomyces corchorushii*, though it seems to have no effect on human α-amylase (Hirayama et al., 1987). However, it can be significant in investigating the variations in human and animal α-amylases because it has an almost identical binding segment to the mammalian α-amylase inhibitor, Tendamistat (Hirayama et al., 1987). Haim is derived from *Streptomyces griseosporeus* and has similar binding characteristics to Tendamistat (Yoshlda et al., 1990). Z-2686 and T-76 are derived from *Streptomyces parvullus* and *Streptomyces mitrosporeus* respectively and contain the triplet which helps in their inhibition of mammalian α-amylase (Hofmann et al, 1985 and Sumitani et al., 1993). AI-409, from *Streptomyces chartreuses*, exhibits inhibition of human salivary α-amylase (Katsuyama et al., 1992).

Tendamistat, which is derived from *Streptomyces tendae*, has also revealed inhibitory properties with α-amylase (Wiegand et al., 1995). Figure 2 shows the structure of Tendamistat. Tendamistat forms a strong stoichiometric 1:1 complex with α-

amylase ("Tendamistat"). Against porcine pancreatic α-amylase, Tendamistat has an inhibitory constant of 9 x 10^{-12} M (Wiegand et al., 1995). Tendamistat is a fairly large molecule, 74 amino acids long, containing six beta sheets and two disulfide bonds between Cystine[11]-Cystine[27] and Cystine[45]-Cystine[73] ("Tendamistat"). Some studies have concluded that its activity is linked to these intact disulfide bonds (Vertesy et al., 1984). One of these disulfide bridges stabilizes two antiparallel β-strands which connects the β-loop containing the triplet tryptophan[18], arginine[19], and tyrosine[20] (Wiegand et al., 1995). This triplet is essential in binding with α-amylase.

Figure 2. Three-Dimensional Model of the Structure of Tendamistat. (Dall'Antonia.)

Four segments of Tendamistat are involved in binding with α-amylase (Wiegand et al., 1995). The Tendamistat- α-amylase complex is found in Figure 3. Segment 1 contains the triplet tryptophan[18], arginine[19], and tyrosine[20] and the residue tyrosine[15] (Wiegand et al., 1995). Hydrogen bonds are formed between this segment of Tendamistat and α-amylase. In the active site of porcine pancreatic α-amylase, three residues, aspartic acid[197], glutamic acid[233], and aspartic acid[300], have been suggested as

the catalytic residues (Wiegand et al., 1995). Arginine[19] of Tendamistat forms a salt bridge with glutamic acid[233] of α-amylase (Wiegand et al., 1995). Segment 2 contains leucine[44] and tyrosine[46], which form hydrophobic interactions and hydrogen bonding with α-amylase, and this segment is stabilized by one of the disulfide bonds (Wiegand et al., 1995). Segment 3 binds to α-amylase through hydrophobic interactions and contains the amino acids: glutamine[52], isoleucine[53], threonine[54], and threonine[55] (Wiegand et al., 1995). Segment 4 connects the two β-sheets of the β-barrel and stabilizes the triplet 18-20 (Wiegand et al., 1995). All the segments of Tendamistat and the corresponding interactions with α-amylase can be found in Table 1.

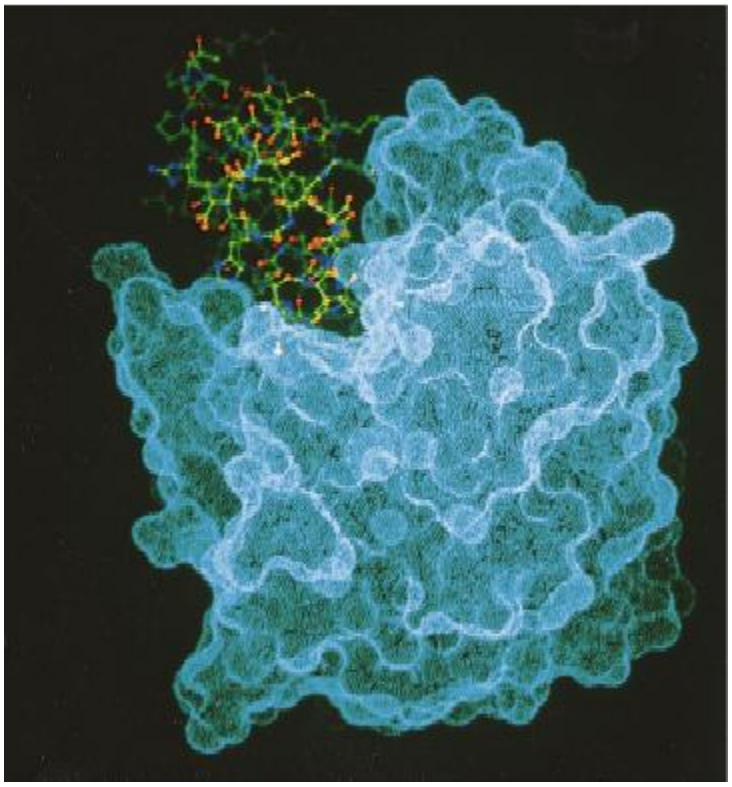

Figure 3. Tendamistat - α-Amylase complex (Wiegand et al.)

Table 1. Amino acid residues in the binding segments of the Tendamistat- α-amylase complex (Wiegand et al., 1995).

Segment	Tendamistat	Porcine Pancreatic α-amylase	Polar Interactions	Contact Area (Å^2)
1	Trp^{18}, Arg^{19}, Tyr^{20}, Tyr^{15}	Trp^{58}, Trp^{59}, Tyr^{62}, Val^{63}, Lys^{200}, His^{201}, Glu^{233}, Ile^{235}, His^{305}, Gly^{309}, Ser^{310}	Tyr^{15} OH – Ser^{310} OG	501
			Arg^{19} NH1 – Glu^{233} OE2	
			Arg^{19} NH2 – Glu^{233} OE1	
			Tyr^{20} OH – His^{201} NE2	
2	Leu^{44}, Tyr^{46}	Glu^{149}, Ser^{150}, Tyr^{151}, Asn^{152}	Tyr^{46} OH – Tyr^{151} N	229
3	Gln^{52}, Ile^{53}, Thr^{54}, Thr^{55}	Tyr^{151}, Leu^{237}, Gly^{238}, Gly^{239}, Glu^{240}	Ile^{53} O – Gly^{238} N	292
			Thr^{54} OG1 – Gly^{239} N	
			Thr^{55} – OG1 – Glu^{240} OE1	
4	Asp^{58}, Gly^{59}, Tyr^{60}, Ile^{61}, Gly^{62}	Trp^{59}, Val^{163}, Asp^{356}	Tyr^{60} OH – Trp^{59} NE1	308
			Tyr^{60} OH – Asp^{356} OD1	

However, there are many drawbacks to using such a larger molecule as a drug. First, larger molecules are more likely to trigger a response from the immune system. Second, natural proteins tend to be inactive by the time they get to their target because they are more likely to be substrates for digestive enzymes. Even though Tendamistat is fairly resistant to hydrolases and does not denature at body temperature, the inclusion of unnatural amino acids would inhibit degradation (Vertesy et al., 1984). Another reason is that it is more expensive to synthesize larger proteins and this is impractical for drug synthesis. Lastly, short sequences are easier to duplicate and be studied.

Through this research, the hope is to find a smaller but similar peptide that can produce the same inhibitory results. A smaller compound, complementary to the active site of Tendamistat, which is amino acids 15-22: Tyrosine – Glutamine– Serine – Tryptophan –Arginine – Tyrosine – Serine – Glutamine (Tyr-Gln-Ser-Trp-Arg-Tyr-Ser-Gln), was used as the parent compound and several variations of it were synthesized. The parent compound has an inhibitory constant of 322 μM (Heyl et al., 2005). The first

variation was replacing tyrosine[15] (Figure 4) with a phenylalanine (Phe) residue (Figure 5) to test for the necessity of the phenolic-OH group on the Tyr residue, which is hydrogen bonded to the glutamine residue in a turn. The rest of the variations were to test for a varied electronic character and pKa for the Tyr[15] by replacing it with a meta-tyrosine (m-Tyr) (Figure 6), a 3,5-dibromotyrosine (DBT) (Figure 7), and 2,6-dimethyltyrosine (DMT) (Figure 8) . Tyrosine has a phenolic pKa of 9.10. Meta-tyrosine's phenolic pKa is 9.69. 3,5-dibromotyrosine has phenolic pKa of 7.21. The phenolic pKa of 2,6-dimethyltyrosine is 10.51.

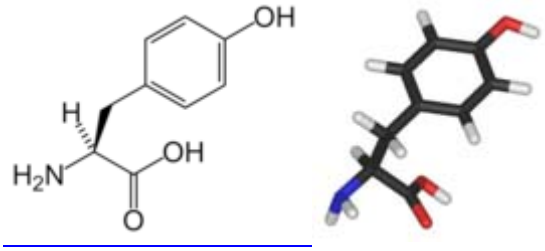

Figure 4. The chemical and 3-D structure of Tyrosine ("Tyrosine").

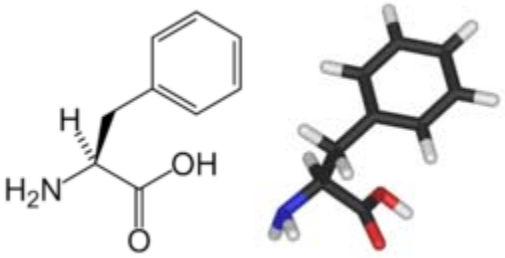

Figure 5. The chemical and 3-D structure of Phenylalanine ("Phenylalanine").

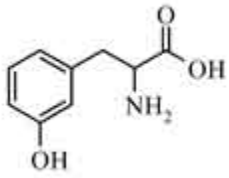

Figure 6. The chemical structure of Meta-Tyrosine ("Meta-Tyrosine").

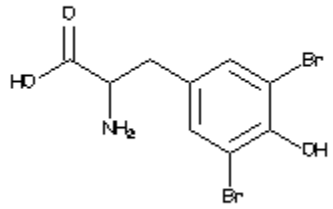

Figure 7. The Structure of 3,5-Dibromotyrosine ("3,5-Dibromotyrosine").

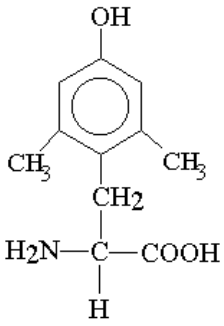

Figure 8. The Structure of 2,6-Dimethyltyrosine

Methods

First, each of the four peptide sequences was synthesized. 0.4 millimoles of each of the amino acids (Bachem, Anaspec, and Synthetech) in the sequence were weighed out and transferred to separate vials with approximately 0.4 millimoles of O-benzotriazol-1-yl-1,1,3,3-tetramethyluronium hexafluorophosphate (HBTU, Bachem), which is used as a coupling agent. The vials were loaded into a Protein Technologies PS3 Automated Protein Synthesizer in the sequence from C-terminus to N-terminus. A vial of two milliliters of Aldrich Chemical Company acetic anhydride was loaded into the synthesizer two slots away from the N-terminus to acetylate the amino group and keep the N-terminus of the peptide uncharged. 0.1 millimole of Fmoc-Rink Amide MBHA resin (Bachem N-α-fluoronylmethyloxycarbonyl Rink amide p-methylbenzyhydylamine resin, which cleaves to an uncharged C-terminus) was weighed into a vessel. A small amount of Aldrich Chemical Company N,N-dimethyl-formamide (DMF) was placed into the reaction vessel before it was connected to the synthesizer.

The basic steps of the peptide synthesis process that was used can be found in Figure 9. The synthesizer started by adding DMF to cause the resin to swell. Then Aldrich Chemical Company 20% piperidine in DMF is added to deprotect the amino acid (remove the Fmoc group) and again DMF is added to wash the resin. The synthesizer then used 0.4M N,N Diisopropylethylamine (DIEA)/DMF to cause the HBTU to form an ester and react with the incoming amino acid. The first amino acid attached to the resin and the subsequent amino acids attached to the N-terminus end of the peptide chain. Last, the DMF again washed the resin. This process repeated as amino acids were added

to the peptide. The last amino acid was just deprotected and the acetic anhydride was mixed in last to acetylate the N-terminus.

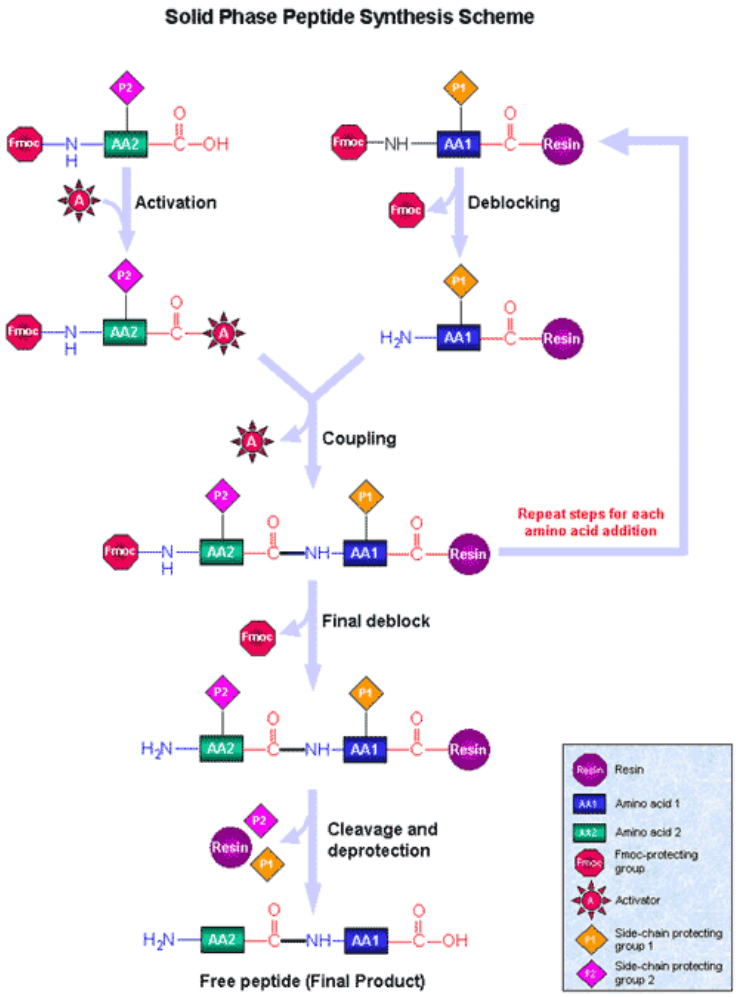

Figure 9. Basic Steps in Solid Phase Peptide Synthesis Using Fmoc-Chemistry ("Basic Steps..")

Next, the peptide was cleaved from the resin and worked up. The resin was placed in a fifteen milliliter fitted disc Buchner funnel vacuum filtration system. The reaction vessel was rinsed with DMF to ensure all the resin was transferred. The resin was then rinsed with methylene chloride to help dry the resin and the resin was left to dry for approximately twenty minutes. A cocktail was created with 0.5 milliliters of anisole,

0.5 milliliters of distilled water, 0.5 milliliters of thioanisole, one crystal phenol, and ten milliliters of trifluoroacetic acid in a twenty milliliter beaker and kept stirring on ice. The anisole, thiosanisole, and phenol are used as scavengers to ensure that the cations pulled off the amino acid chain would not reattach, and the trifluoroacetic acid (TFA) was used to cleave the peptide from the resin. The resin was transferred to the beaker, covered, and stirred for one and a half to two hours. The bright yellow solution changed to a dark brown within twenty minutes. Again the filtration system was setup, but with a fine filter and the beaker was rinsed several times with TFA. The peptide solution was collected in the flask and approximately fifty milliliters of cold diethyl ether was added slowly to the TFA solution containing the peptide to precipitate the peptide. The peptide solution was filtered to remove the diethyl ether and small amounts of ether were added while the peptide was stirred with a spatula to remove the anisole and thioanisole. All the solvents were purchased from Fisher Scientific and Aldrich Chemical Company. After drying for a few minutes, the peptide was transferred to a small lyophilization flask and dissolved in a small amount of 70% acetonitrile in water. An equal volume of distilled water was added and the mixture was frozen by rotating in dry ice/acetone bath. The mixture was then lyophilized overnight on a Virtis Sentry Lyophilizer.

Next to purify the crude peptide, preparative reversed-phase high performance liquid chromatography (HPLC) was performed on Waters 501 HPLC Pumps with a Phenomenex C18 column (2.2 x 25.0 centimeters)(set at 10 milliliters per minute) and a Waters 484 Tunable Absorbance Detector and Waters Automated Gradient Controller. The peptide was massed and transferred to a vial. It was dissolved in DMF and was injected into the HPLC machine with a Waters U6K injector syringe. A linear gradient of

10% to 50% acetonitrile (0.1% TFA)/water (0.1% TFA) was completed over a period of two hours. The basic setup of the HPLC used can be found in Figure 10 with solvent A being the water solution and the solvent B being the acetonitrile solution. When the absorbance peaked, the solution was collected into test tubes. The contents of those tubes were transferred to a small lyophilizer flask and lyophilized overnight. An analytical HPLC was performed to determine the purity of the peptide by injecting a very small amount of the peptide into the HPLC, using the same procedure except that a smaller column was used, with a flow rate of one milliliter per minute, and it was not collected at the end.

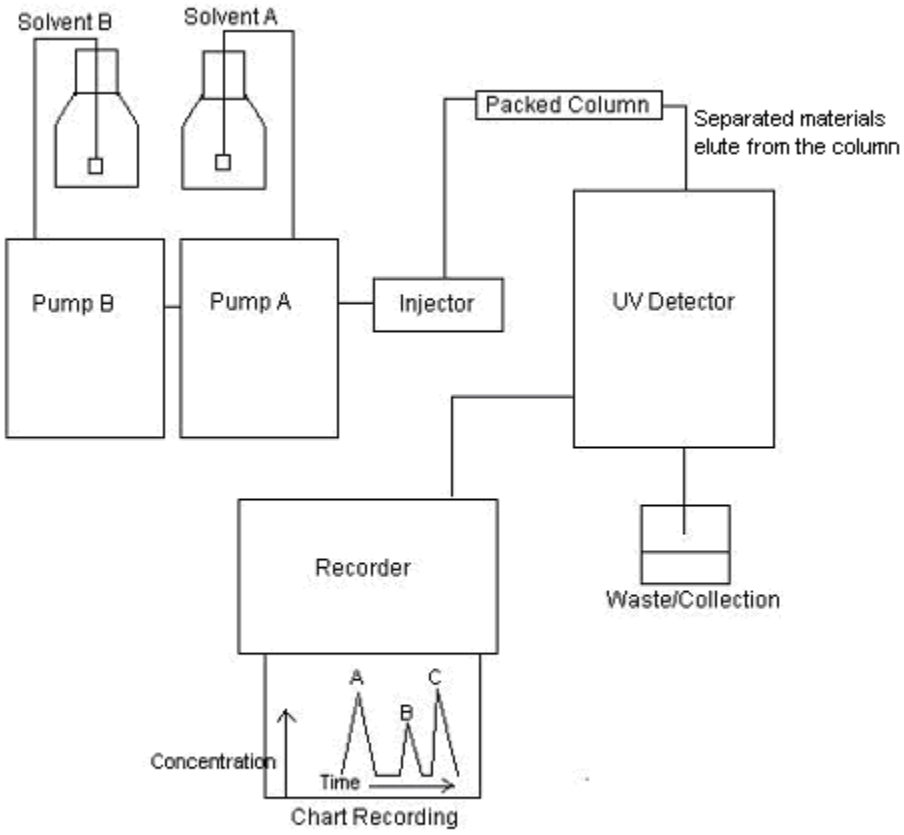

Figure 10. The setup of HPLC used.

Last, three assays were performed to determine enzymatic inhibitory activity. Each of the three assays was performed the same way except for varying the inhibitor concentration which was approximately 0.1 millimolar, 0.2 millimolar, and 0.3 millimolar. Fourteen tubes, seven inhibited and seven uninhibited, were constructed with varying amounts of the porcine pancreatic α-amylase substrate, p-nitrophenyl-α-D-maltoside (Sigma), and 0.025 M Hepes (N-2-hydroxyethylpiperazine-N'-2-ethanesulfonic acid) buffer. Porcine pancreatic α-amylase is used as the enzyme because of its similarity to human α-amylase. Porcine pancreatic α-amylase contains eighteen of the twenty-one amino acids in the binding sequences (Wiegand et al., 1995). The enzyme, porcine pancreatic α-amylase, and inhibitor (the peptide in DMSO), or the substitution for uninhibited tubes which was Aldrich Chemical Company dimethylsulfoxide (DMSO) volumes remained constant. All of the volumes added to the tubes can be found in Table 2. The substrate was prepared by dissolving it in Hepes buffer to make a fifty millimolar solution. The enzyme was also prepared by dissolving forty-six microliters of porcine pancreatic α-amylase in 454 microliters of Hepes buffer. The inhibitor was prepared by dissolving approximately three milligrams, two milligrams, and one milligrams of peptide in 1400 microliters of DMSO to make approximately 0.3 millimolar, 0.2 millimolar, and 0.1 millimolar solutions (when diluted in the test tubes) respectively. DMSO was used instead of water because it was previously found that there was poor solubility of Tendamistat based peptides in water (Selfer et al., 1997), and the DMSO did not influence the reaction based on earlier control studies.

Table 2. Total volume of solutions added to the tubes.

Tube	Substrate Volume (μL)	Buffer Volume (μL)	Enzyme Volume (μL)	DMSO or Inhibitor Volume (μL)
1	20	783.9	29.4	166.7
2	60	743.9	29.4	166.7
3	100	703.9	29.4	166.7
4	160	643.9	29.4	166.7
5	200	603.9	29.4	166.7
6	260	543.9	29.4	166.7
7	320	483.9	29.4	166.7

The enzyme was added first to the tubes, followed by the HEPES buffer, and then the inhibitor or DMSO depending on the tube. The tubes were incubated at 30^{o}C for a half hour. The substrate was added immediately before the solution was placed in the Beckman DU 246 UV/VIS spectrophotometer set at 405 nanometers. This wavelength was chosen because this is where the yellow substrate product, p-nitrophenolate ion, absorbs light. The spectrophotometer was set to record the change in absorbance over a two minute time period at intervals of ten seconds. The absorbance-based rates were converted to concentration-based initial velocities by using Beer's Law. The rates of absorbance over time were recorded and data analysis using Michaelis-Menten and Lineweaver-Burk plots created on Microsoft Excel.

Results and Discussion

Phe Modification

The following tables (Tables 3-5) contain the rates of absorbance over time for the three assays performed with the Phe modification. When the enzyme-substrate complex is formed, a yellow color is produced. In all Phe modification assays, the uninhibited tubes produced the yellow color, while all of the inhibited tubes remained clear in color. Michaelis-Menten and Lineweaver-Burk plots for the three assays were created using this data, which can be found in Figures 11-16. The plots were created using a concentration based rate, corrected with Beer's Law. From the Lineweaver-Burk plot, the V_{max}, K_m, and K_i were determined and can be found in Table 6. The average K_i was calculated to be 1248 μM. An overall K_i was also determined using the slopes of the Lineweaver-Burk plots. When all three slopes were plotted, the slope of the line of best fit was negative and would produce a negative K_i value, so the point which caused the line to become negative was removed. Figure 17 shows the plot without the outlier slope, which produced a K_i value of 35.9 μM.

Table 3. Rates for the assay of the 0.26 mM Phe modification.

Tube	Concentration of Substrate (mM)	Rate of Uninhibited (dA/min)	Rate of Inhibited (dA/min)
1	0.94	0.0028	0.0026
2	2.8	0.0061	0.0076
3	4.7	0.0254	0.0156
4	7.5	0.0170	0.157
5	9.4	0.0195	0.0168
6	12.2	0.0201	0.0183
7	15.0	0.0222	0.0213

Table 4. Rates of the assay of the 0.13 mM Phe modification.

Tube	Concentration of Substrate (mM)	Rate of Uninhibited (dA/min)	Rate of Inhibited (dA/min)
1	0.94	0.0032	0.0020
2	2.8	0.0198	0.0077
3	4.7	0.0105	0.0111
4	7.5	0.0143	0.0150
5	9.4	0.0151	0.0128
6	12.2	0.0177	0.0166
7	15.0	0.0160	0.0161

Table 5. Rates of the assay of the 0.065 mM Phe modification.

Tube	Concentration of Substrate (mM)	Rate of Uninhibited (dA/min)	Rate of Inhibited (dA/min)
1	0.94	0.0007	0.0019
2	2.8	0.0030	0.0031
3	4.7	0.0056	0.0042
4	7.5	0.0076	0.0052
5	9.4	0.0057	0.0059
6	12.2	0.0081	0.0070
7	15.0	0.0054	0.0080

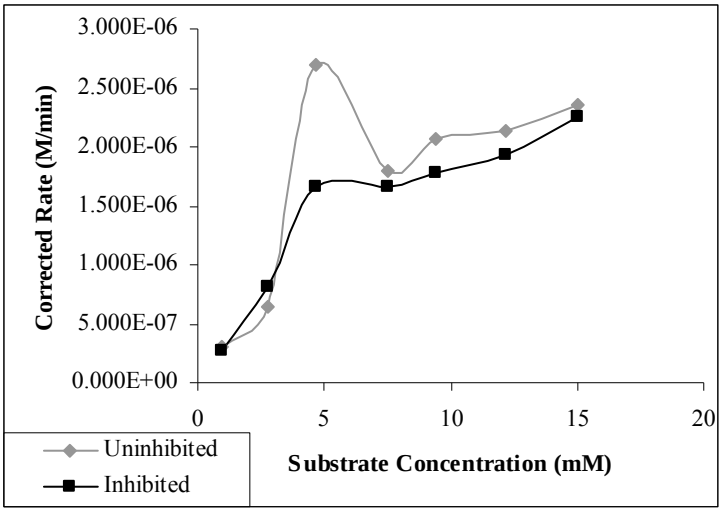

Figure 11. Michaelis-Menten plot for the assay of the 0.26 mM of Phe modification.

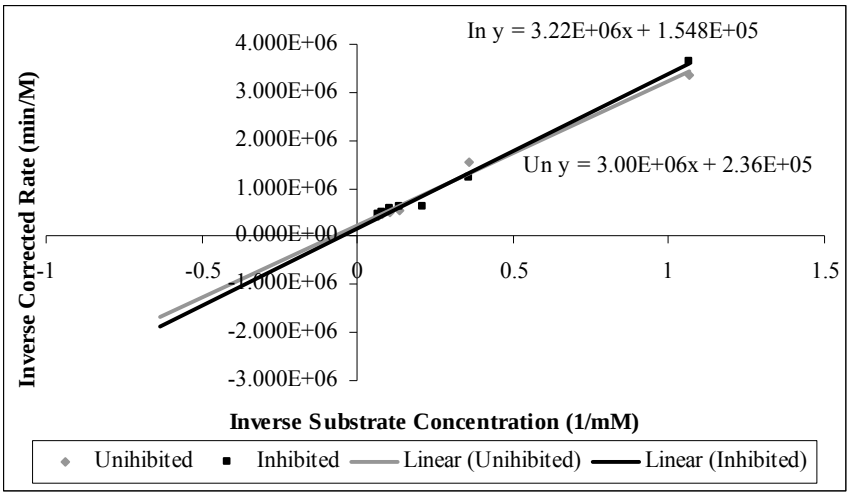

Figure 12. Lineweaver-Burk plot for the assay of the 0.26 mM Phe modification.

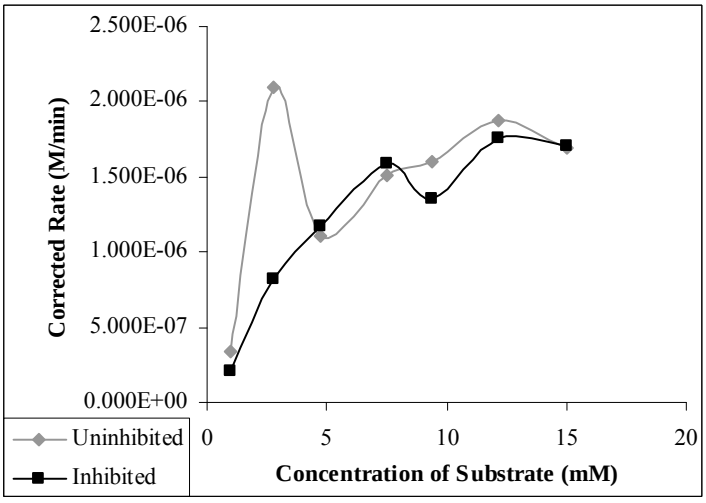

Figure 13. Michaelis-Menten plot for the assay of the 0.13 mM Phe modification.

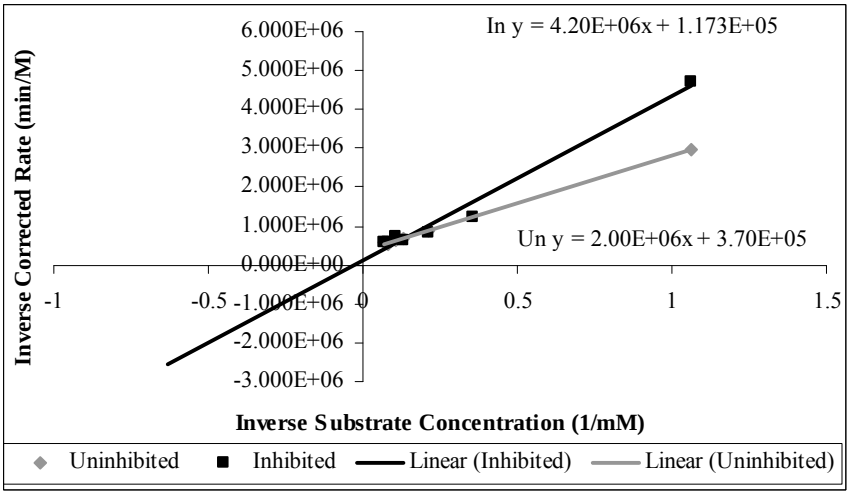

Figure 14. Lineweaver-Burk plot for the assay of the 0.13 mM Phe modification

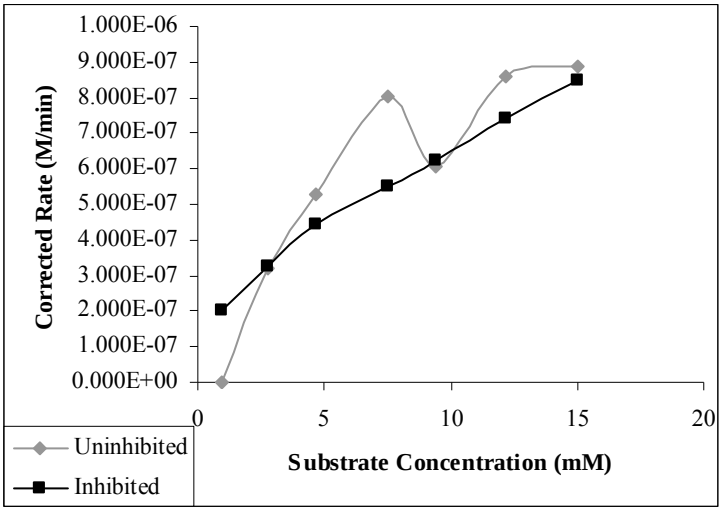

Figure 15. Michaelis-Menten plot for the assay of the 0.065 mM Phe modification.

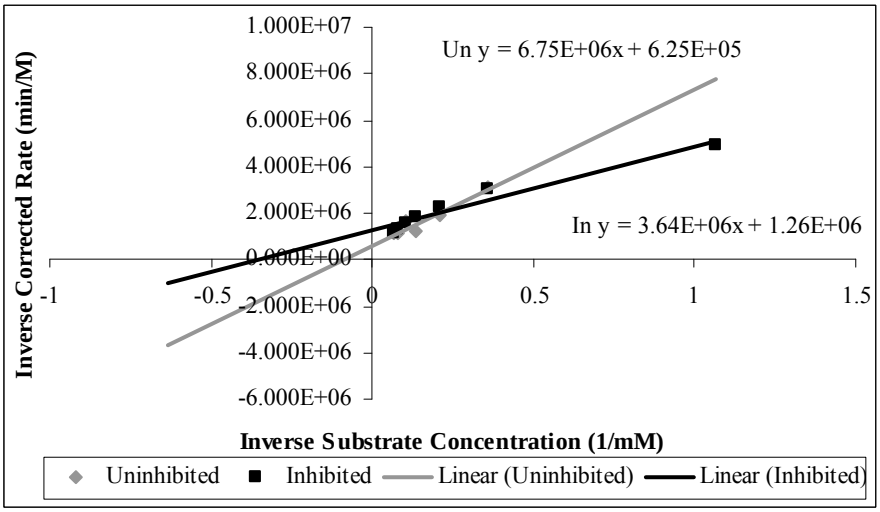

Figure 16. Lineweaver-Burk plot for the assay of the 0.065 mM Phe modification.

Table 6. The V_{max}, K_m, and K_i for all three Phe modification assays.

Inhibitor Concentration (mM)	V_{max}(M/min) inhibited	K_m(mM) inhibited	V_{max}(M/min) uninhibited	K_m(mM) uninhibited	K_i(μM)
0.26	6.460×10^{-6}	20.16	4.235×10^{-6}	12.71	3550
0.13	8.525×10^{-6}	35.80	2.702×10^{-6}	6.544	118
0.065	7.924×10^{-7}	2.885	1.599×10^{-6}	10.79	76.2

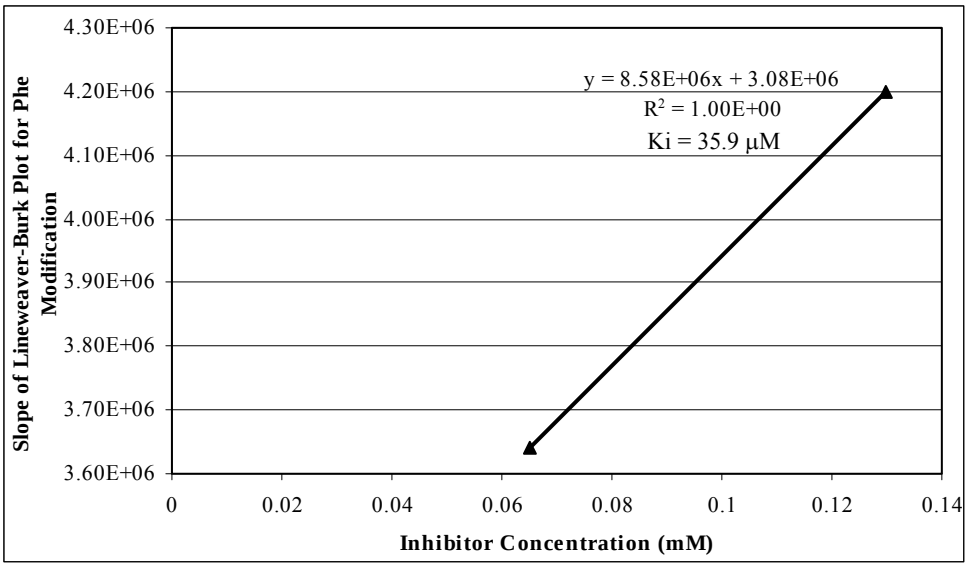

Figure 17. K_i determination with two Phe modification slopes versus the inhibitor concentration.

m-Tyr Modification

Tables 7 through 9 contain the rates of absorbance over time for the 0.25mM, 0.2mM, and the 0.08mM m-Tyr modification assays performed. Like the Phe modification assays, the m-Tyr assays' uninhibited tubes produced the yellow color while all of the inhibited tubes remained clear in color. Figures 18-23 show the Michaelis-Menten and Lineweaver-Burk plots for the three assays, created using this data. Again from the Lineweaver-Burk plot, the V_{max}, K_m, and K_i were determined and can be found in Table 10. The average K_i was 116.5 μM (the third assay K_i was not used due to the poor rates). An overall K_i was also determined using the slopes of the Lineweaver-Burk plots. Again after plotting all three slopes, a negative K_i was obtained, so the outlier slope was discarded. Figure 24 shows the plot without the outlier slope, which produced a K_i value of 192 μM.

Table 7. Rates for the assay of the 0.25 mM m-Tyr modification.

Tube	Concentration of Substrate (mM)	Rate of Uninhibited (dA/min)	Rate of Inhibited (dA/min)
1	0.94	-0.0017	0.0003
2	2.8	0.0001	0.0020
3	4.7	-0.0001	0.0039
4	7.5	0.0016	0.0065
5	9.4	0.0008	0.0054
6	12.2	0.0015	0.0046
7	15.0	0.0009	0.0038

Table 8. Rates of the assay of the 0.2 mM m-Tyr modification.

Tube	Concentration of Substrate (mM)	Rate of Uninhibited (dA/min)	Rate of Inhibited (dA/min)
1	0.94	0.0022	0.0009
2	2.8	0.0008	0.0021
3	4.7	0.0029	0.0024
4	7.5	0.0013	0.0038
5	9.4	0.0010	0.0035
6	12.2	0.0005	0.0032
7	15.0	0.0003	0.0059

Table 9. Rates of the assay of the 0.08 mM m-Tyr modification.

Tube	Concentration of Substrate (mM)	Rate of Uninhibited (dA/min)	Rate of Inhibited (dA/min)
1	0.94	0.0042	0.0009
2	2.8	-0.0003	0.0008
3	4.7	0.0005	-0.0009
4	7.5	0.0004	-0.0010
5	9.4	-0.0015	-0.0003
6	12.2	-0.0027	-0.0012
7	15.0	-0.0003	-0.0030

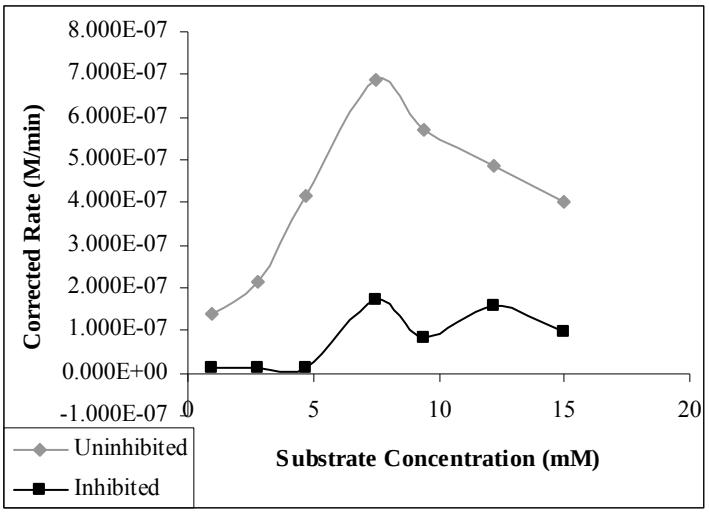

Figure 18 Michaelis-Menten plot for the assay of the 0.25 mM m-Tyr modification.

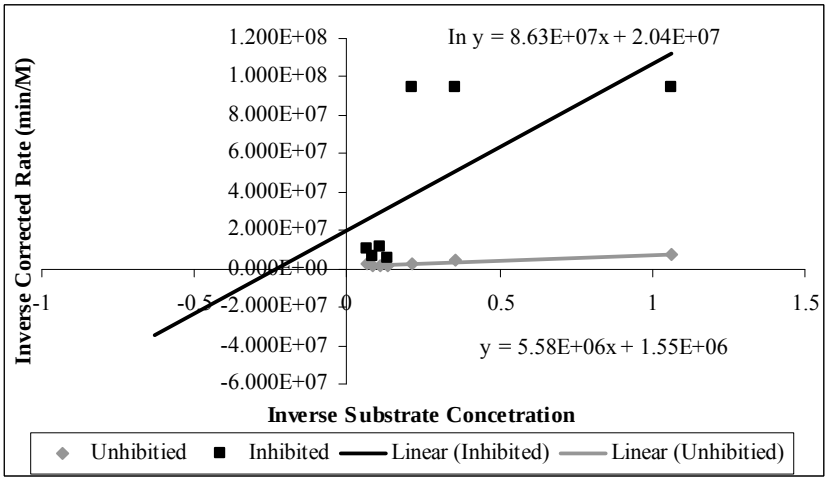

Figure 19 Lineweaver-Burk plot for the assay of the 0.25 mM m-Tyr modification.

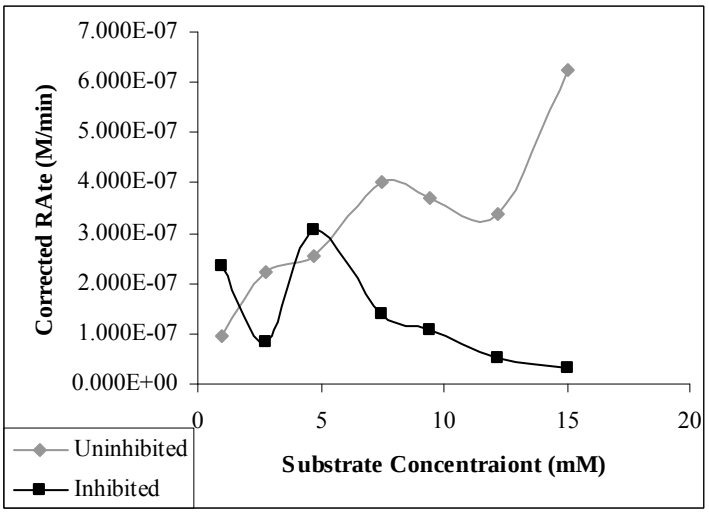

Figure 20. Michaelis-Menten plot for the assay of the 0.20 mM m-Tyr modification.

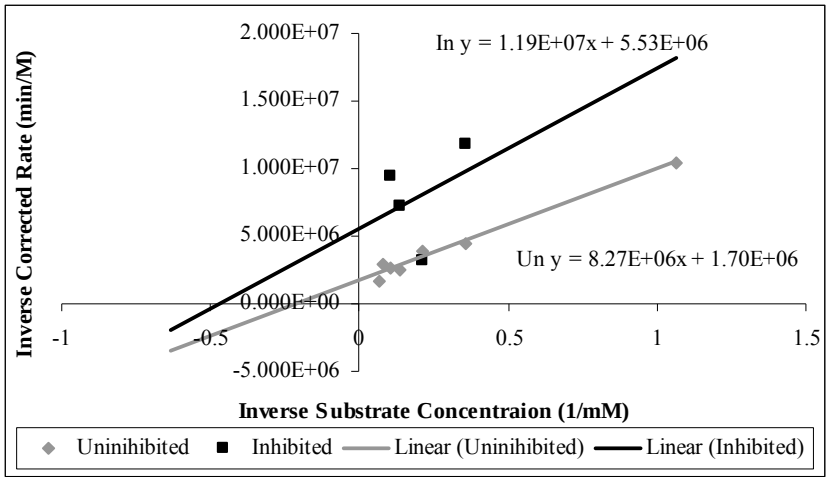

Figure 21. Lineweaver-Burk plot for the assay of the 0.20 mM m-Tyr modification

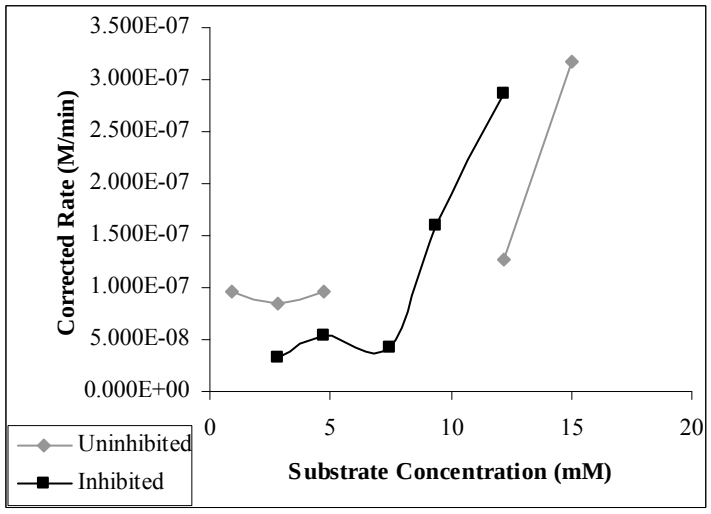

Figure 22. Michaelis-Menten plot for the assay of the 0.08 mM m-Tyr modification.

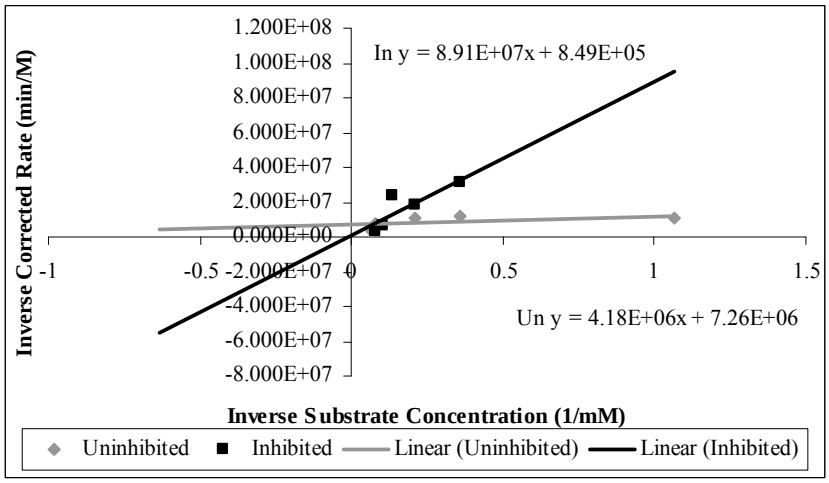

Figure 23. Lineweaver-Burk plot for the assay of the 0.08 mM m-Tyr modification.

Table 10. The V_{max}, K_m, and K_i for all three m-Tyr modification assays.

Inhibitor Concentration (mM)	V_{max}(M/min) inhibited	K_m(mM) inhibited	V_{max}(M/min) uninhibited	K_m(mM) uninhibited	K_i(μM)
0.25	4.897×10^{-8}	4.228	6.450×10^{-7}	3.598	187
0.20	1.807×10^{-7}	2.144	5.875×10^{-7}	4.857	46
0.08	1.178×10^{-6}	-104.9	1.377×10^{-7}	3.012	2.537×10^{5}

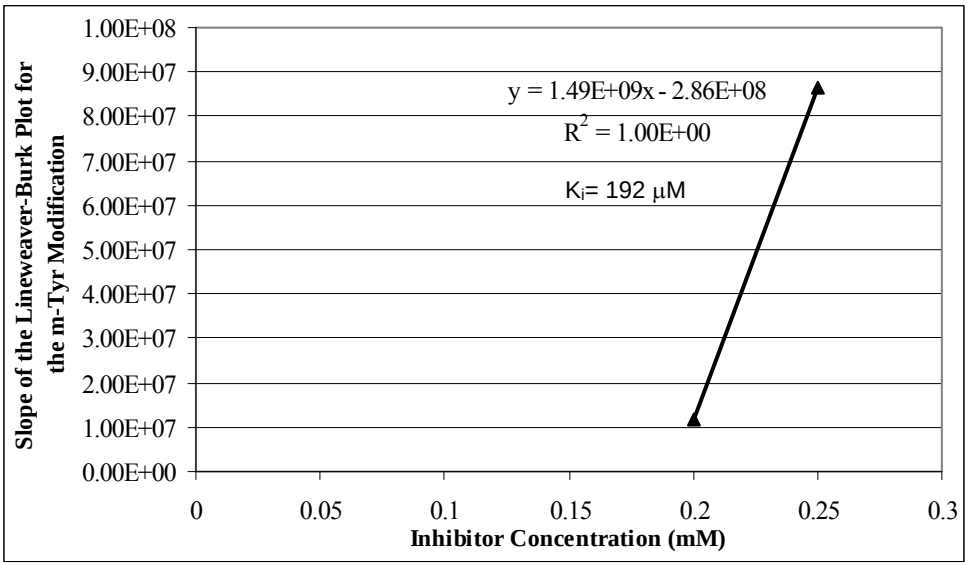

Figure 24. K_i determination with two m-Tyr modification slopes versus the inhibitor concentration.

DBT Modification

The rates of absorbance over time for the three DBT modification assays performed are found in Tables 11-13. The assays uninhibited tubes produced a deeper yellow color while all of the inhibited tubes were less yellow in color. Figures 25-30 show the Michaelis-Menten and Lineweaver-Burk plots for the three assays. Table 14 shows the V_{max}, K_m, and K_i that were determined from the Lineweaver-Burk plots. 32.67 μM was calculated to be the average K_i value for the DBT modification. Again the overall K_i was determined using the slopes of the Lineweaver-Burk plots. To be consistent with the modifications, an outlier point was omitted from the plot of the three

slopes. A K_i value of 78.2 μM was produced from the plot without the outlier slope, shown in Figure 31.

Table 11. Rates for the assay of the 0.3 mM DBT modification.

Tube	Concentration of Substrate (mM)	Rate of Uninhibited (dA/min)	Rate of Inhibited (dA/min)
1	0.94	0.0012	-0.0001
2	2.8	0.0046	0.0014
3	4.7	0.0073	0.0004
4	7.5	0.0074	-0.0004
5	9.4	0.0095	0.0020
6	12.2	0.0067	0.0016
7	15.0	0.0135	0.0022

Table 12 Rates of the assay of the 0.2 mM DBT modification.

Tube	Concentration of Substrate (mM)	Rate of Uninhibited (dA/min)	Rate of Inhibited (dA/min)
1	0.94	0.0016	0.0011
2	2.8	0.0015	0.0018
3	4.7	0.0030	0.0010
4	7.5	0.0057	0.0014
5	9.4	0.0075	-0.0008
6	12.2	0.0065	0.0009
7	15.0	0.0074	-0.0030

Table 13 Rates of the assay of the 0.1 mM DBT modification.

Tube	Concentration of Substrate (mM)	Rate of Uninhibited (dA/min)	Rate of Inhibited (dA/min)
1	0.94	0.0033	0.0025
2	2.8	0.0085	0.0044
3	4.7	0.0128	0.0018
4	7.5	0.0173	0.0037
5	9.4	0.0137	0.0031
6	12.2	0.0192	0.0034
7	15.0	0.0194	0.0028

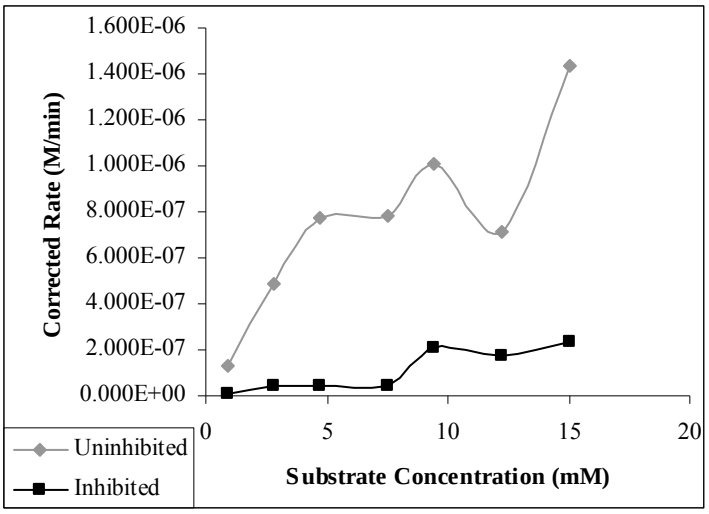

Figure 25. Michaelis-Menten plot for the assay of the 0.30 mM DBT modification.

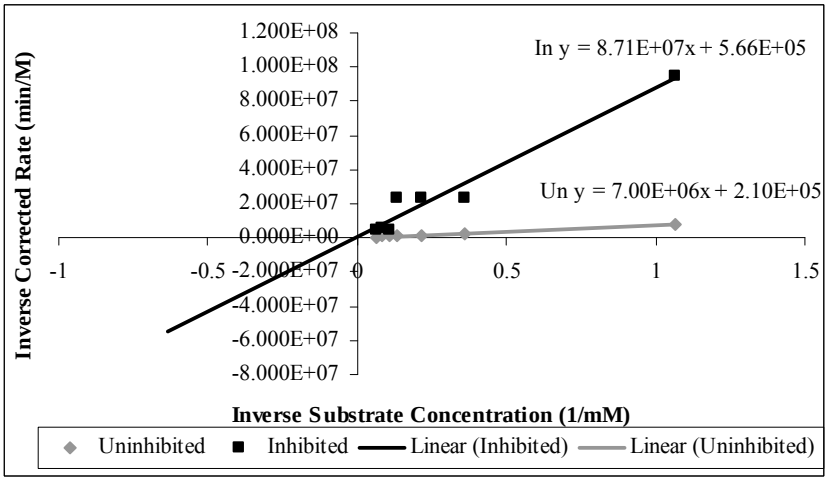

Figure 26. Lineweaver-Burk plot for the assay of the 0.30 mM DBT modification.

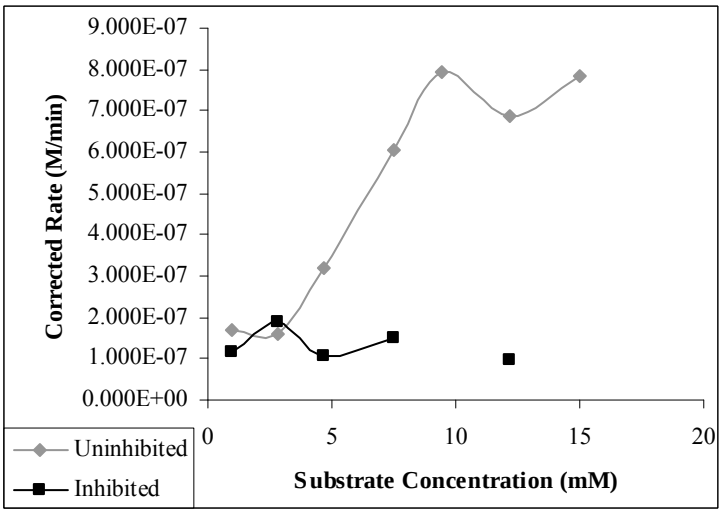

Figure 27. Michaelis-Menten plot for the assay of the 0.20 mM DBT modification.

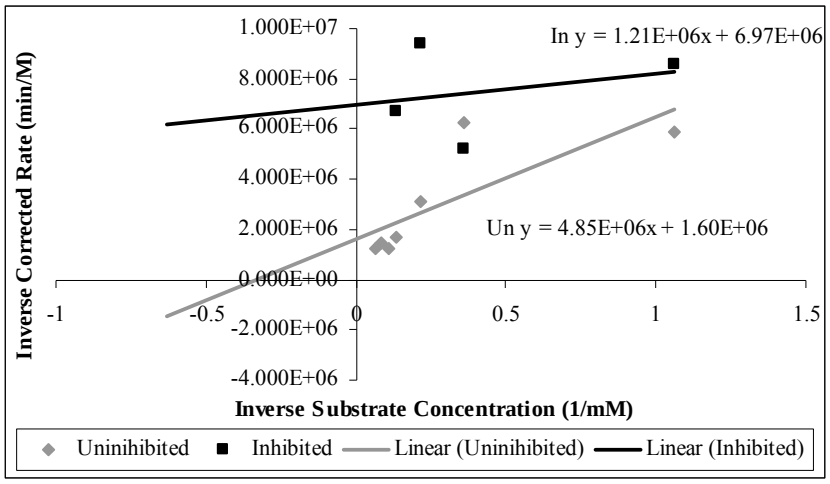

Figure 28. Lineweaver-Burk plot for the assay of the 0.20 mM DBT modification.

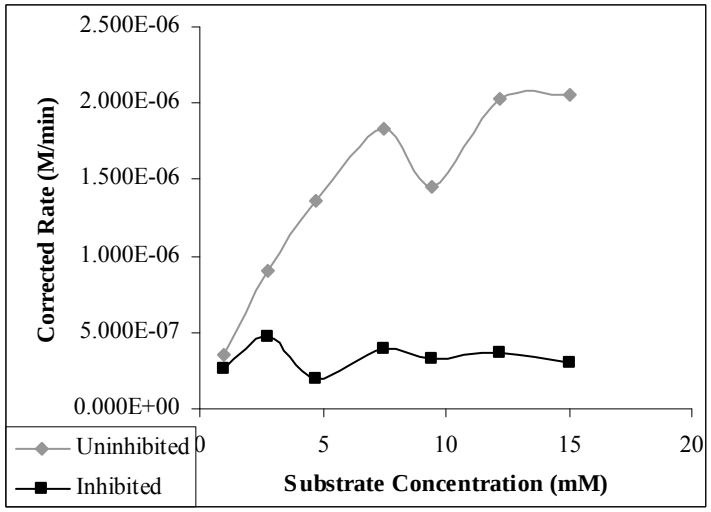

Figure 29. Michaelis-Menten plot for the assay of the 0.10 mM DBT modification.

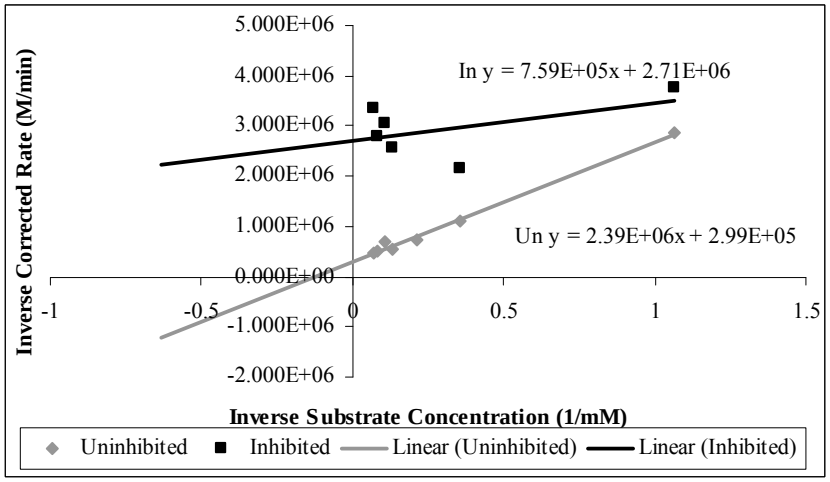

Figure 30. Lineweaver-Burk plot for the assay of the 0.10 mM DBT modification.

Table 14 The V_{max}, K_m, and K_i for all three DBT modification assays.

Inhibitor Concentration (mM)	V_{max}(M/min) inhibited	K_m(mM) inhibited	V_{max}(M/min) uninhibited	K_m(mM) uninhibited	K_i(μM)
0.3	1.767×10^{-6}	153.9	4.762×10^{-6}	332.2	26.2
0.2	1.436×10^{-7}	0.1730	6.270×10^{-7}	3.040	59.4
0.1	3.685×10^{-7}	0.2796	3.344×10^{-7}	7980	12.4

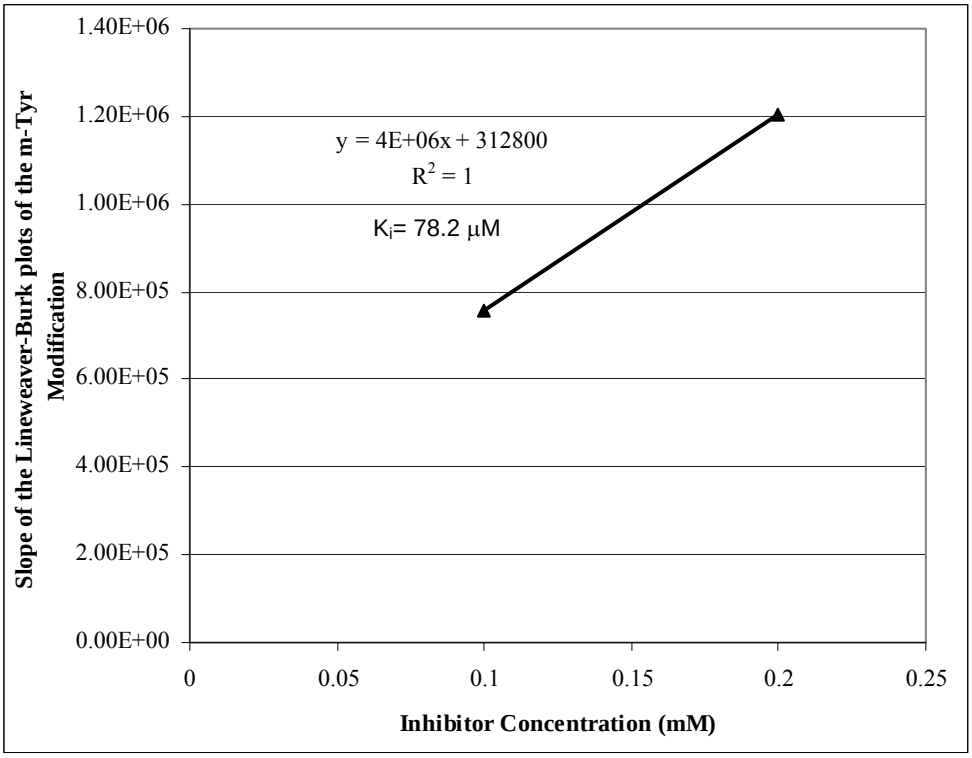

Figure 31. K_i determination with two DBT modification slopes versus the inhibitor concentration.

DMT Modification

Table 15-17 show the rates of absorbance over time for the 0.3 mM, 0.2 mM, and 0.1 mM DMT modification assays performed. Like the other assays, the uninhibited tubes produced a deeper yellow color while all of the inhibited tubes were less yellow in color. The Michaelis-Menten and Lineweaver-Burk plots for the three assays are shown in Figures 32-37. The V_{max}, K_m, and K_i, determined from the Lineweaver-Burk plots, are shown in Table 18. 351.8 μM was calculated to be the average K_i value for the DMT

modification. Again the overall K_i was determined using the slopes of the Lineweaver-Burk plots. A K_i value of 163 μM was produced from the plot without the outlier slope (to be consistent with the other modification) shown in Figure 38.

Table 15. Rates of the assay of the 0.3 mM DMT modification.

Tube	Concentration of Substrate (mM)	Rate of Uninhibited (dA/min)	Rate of Inhibited (dA/min)
1	0.94		
2	2.8	0.0016	0.0025
3	4.7	0.0089	0.0044
4	7.5	0.0027	0.0082
5	9.4	0.0064	0.0056
6	12.2	0.0075	0.0078
7	15.0	0.0079	0.0113

Table 16. Rates of the assay of the 0.2 mM DMT modification.

Tube	Concentration of Substrate (mM)	Rate of Uninhibited (dA/min)	Rate of Inhibited (dA/min)
1	0.94	0.0037	0.0038
2	2.8	0.0056	0.0122
3	4.7	0.0043	0.0098
4	7.5	0.0065	0.0082
5	9.4	0.0090	0.0124
6	12.2	0.0085	0.0181
7	15.0	0.0196	0.0207

Table 17. Rates of the assay of the 0.1 mM DMT modification.

Tube	Concentration of Substrate (mM)	Rate of Uninhibited (dA/min)	Rate of Inhibited (dA/min)
1	0.94	0.0013	0.0016
2	2.8	0.0021	0.0056
3	4.7	0.0090	0.0085
4	7.5	0.0150	0.0108
5	9.4	0.0214	0.0185
6	12.2	0.0153	0.0190
7	15.0	0.0064	0.0142

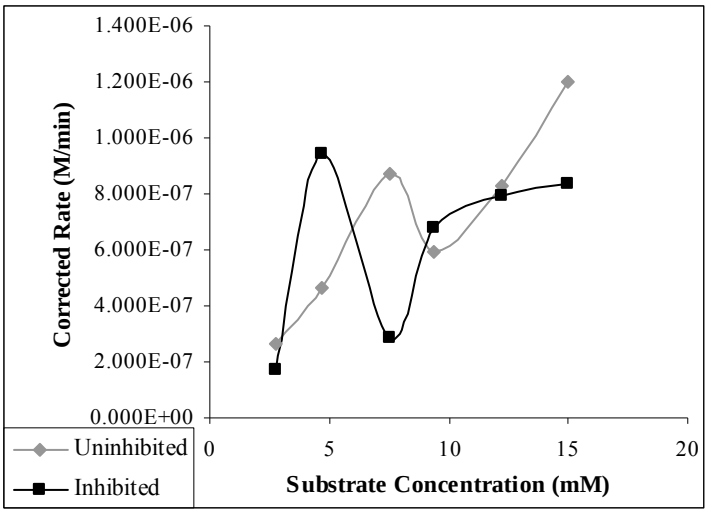

Figure 32. Michaelis-Menten plot for the assay of the 0.30 mM DMT modification.

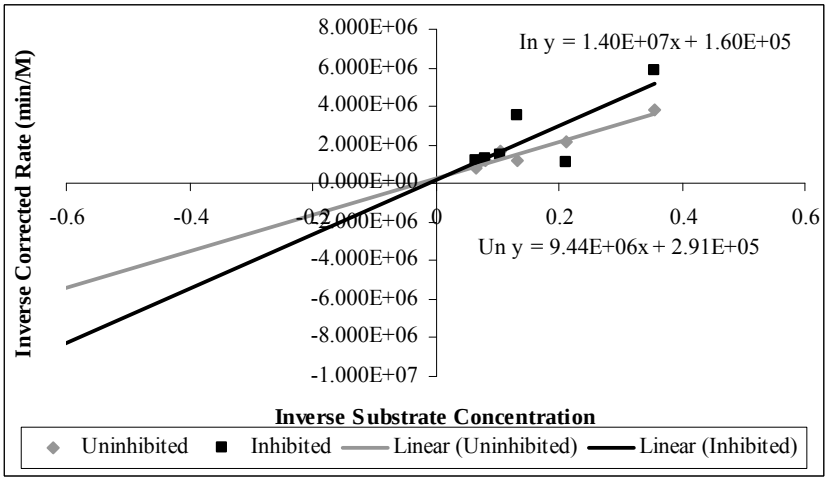

Figure 33. Lineweaver-Burk plot for the assay of the 0.30 mM DMT modification.

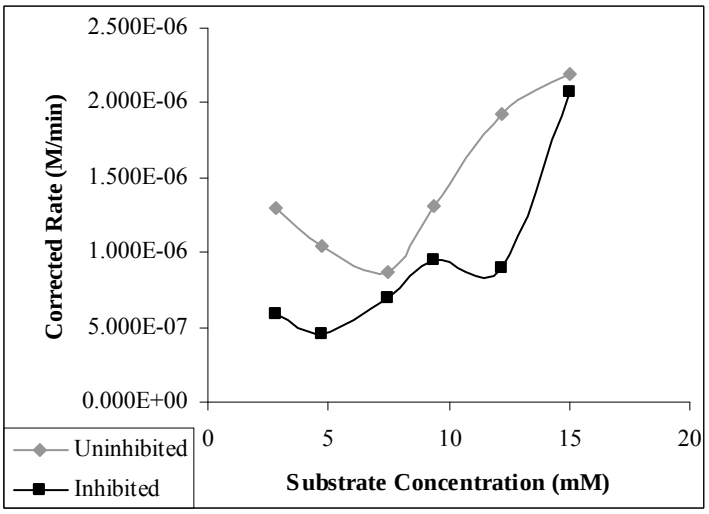

Figure 34. Michaelis-Menten plot for the assay of the 0.20 mM DMT modification.

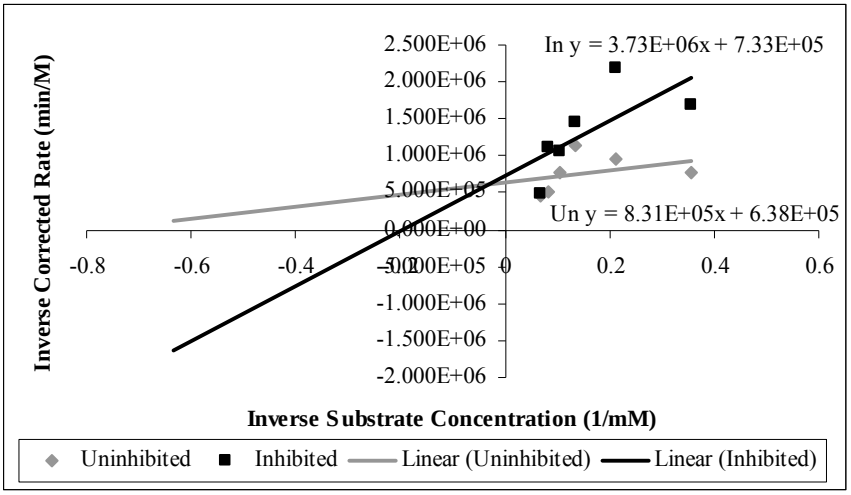

Figure 35. Lineweaver-Burk plot for the assay of the 0.20 mM DMT modification.

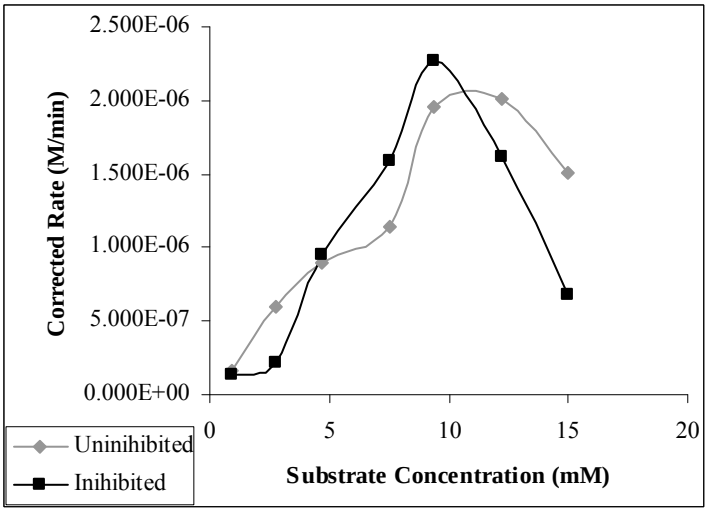

Figure 36. Michaelis-Menten plot for the assay of the 0.10 mM DMT modification.

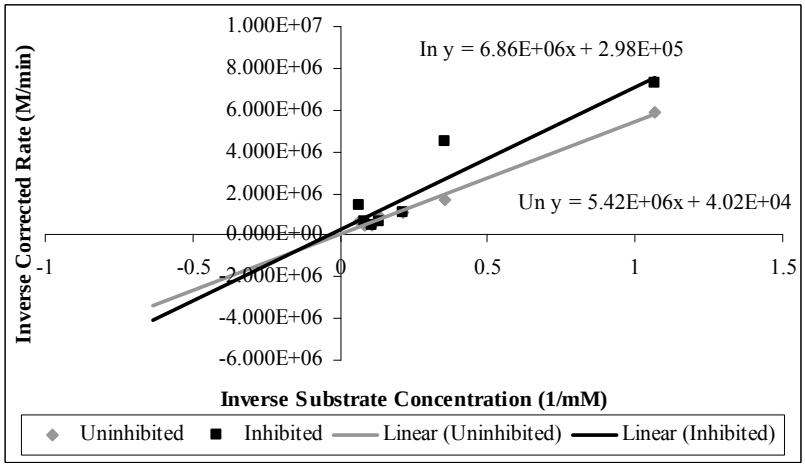

Figure 37. Lineweaver-Burk plot for the assay of the 0.10 mM DMT modification.

Table 18. The V_{max}, K_m, and K_i for all three DMT modification assays.

Inhibitor Concentration (mM)	V_{max}(mM/min) inhibited	K_m(mM) inhibited	V_{max}(mM/min) uninhibited	K_m(mM) uninhibited	K_i(μM)
0.3	7.143E-8	87.72	3.432E-6	32.41	622
0.2	1.364E-6	5.085	1.568E-6	1.303	57.4
0.1	3.351E-6	22.99	2.486E-5	134.7	376

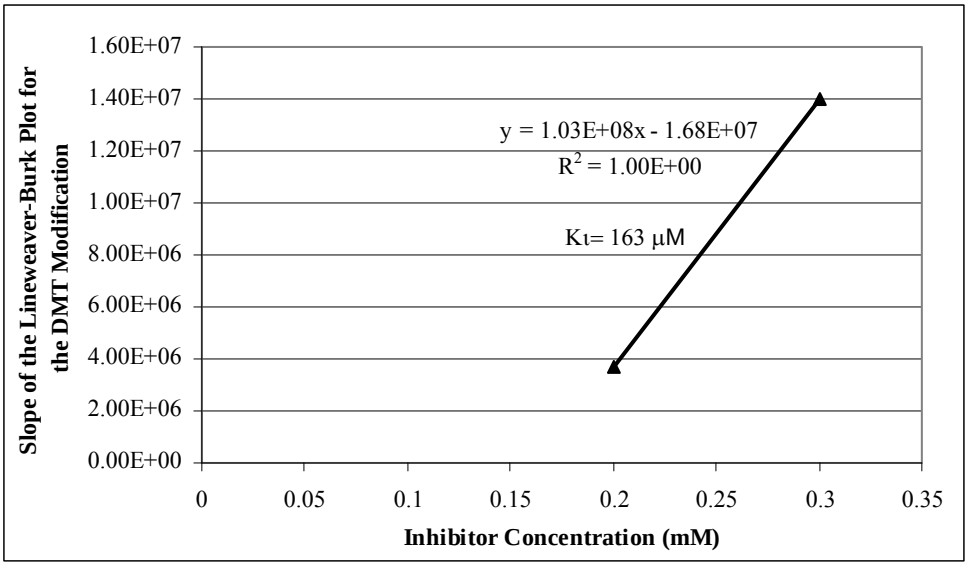

Figure 38. K_i determination with two DMT modification slopes versus the inhibitor concentration.

Along with the four compounds studied in this research, seven other compounds were also studied overall. The data for these compounds is courtesy of Brahmlin Sethi, Michele Lawrence, Carrie Bowen, Lindsay Beitler, Erin Harning, Sreeja Sreekumar, Ayse Hancer, and Steve Fernandes. Table 19 shows the physiochemical and kinetic data for the various compounds. The kinetic data was determined from the assays completed by observing the rate of cleavage of p-nitrophenyl-□-D-maltoside by porcine pancreatic α-amylase. The pKa values were obtained from a study by D. Heyl (2003). The purity of the compounds was determined by RP-HPLC peak integration at 214 nanometers. The K_i values are mean values from conducting three to five assays which accounts for the differences from the previous tables in some of the average K_i values. Since the values

are the results of more runs, they can be considered more reliable and will be used in the discussion. To determine if there was a correlation between the pKa and the inhibitory property of the peptide modification, the pKa was graphed versus the inhibition constant, which can be found in Figure 43.

Table 19. Physiochemical and Kinetic Data for the Peptide Inhibitors

N-terminus of Peptide	Phenolic pKa	Purity (%)	K_i (μM)
Phe	-	97	1270
m-Tyr	-	99	116
p-NH_2-Phe	-	98	595
Tyr	9.10	99	322
3-OH-Tyr	9.69	99	136
3-Cl-Tyr	8.79	98	265
3-I-Tyr	8.81	99	157
3-NO_2-Tyr	7.45	98	147
3,5-diI-Tyr	7.38	98	114
3,5-diBr-Tyr	7.21	99	69.7
2,6-diCH_3-Tyr	10.51	99	376

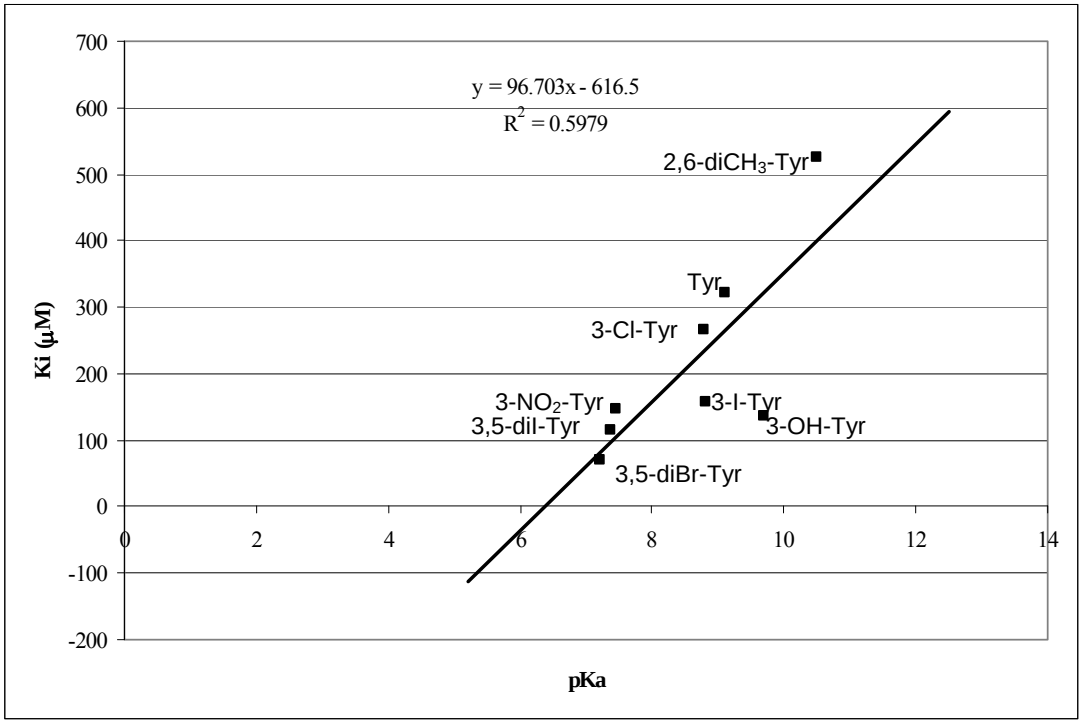

Figure 39. Phenolic pKa of N-Terminal Tyr residue versus the inhibition constant.

Conclusion

From the Ki values for the Phe modification, it would seem that the inhibitor has a lower inhibitory quality than the parent compound, with a K_i value of 1270 μM compared to the parent value of 322 μM. This suggests that the hydroxyl group on the tyrosine, which plays a role in hydrogen bonding, is important either in bonding to α-amylase during the inhibition process or in maintaining the required peptide conformation. The modification m-Tyr produced an average K_i value of 116 μM, slightly better than the parent compound. This suggests that the placement of the hydroxyl group on tyrosine also contributes to the inhibitory quality. Perhaps it is a better location for hydrogen bonding than the natural para-position. The average K_i value for the DBT modification was 69.7 μM, much lower than the parent value of 322μM. DBT also has a lower pKa value, which suggests that the added elements on the tyrosine which decrease the pKa, also increase its ability to hydrogen bind with α-amylase or intramolecularly to stabilize a favorable orientation. The opposite occurs with the DMT modification. An increased pKa from the addition of the methyl groups, compared to the parent compound, is correlated with a decreased inhibitory ability because of a decreased ability to hydrogen bond. The average Ki value for the DMT modification was 376 μM.

From testing the various modifications to the parent compound with varying pKa values, it seems that as the pKa value of the inhibitor increases, the K_i value of the compound also increases. The graph of the pKa of the modification versus the K_i suggests a moderate correlation between the pKa and the inhibitory activity with inhibition improving as pKa decreases and acidic character increases. Since the higher the pKa, the lower the ability to give up the phenolic proton and thus act as a hydrogen

bond donor, it seems that the hydrogen bonding of the hydroxyl group is important in maintaining the shape of the inhibitor and therefore the function of the inhibitor and its ability to bond with α-amylase. Also from running the various modifications, it was determined that competitive inhibition is generally occurring. This indicates the type of interaction that is going on at the active site between the inhibitor and the enzyme.

To obtain better results, more assays with a greater range of inhibitor concentrations should be run in order to verify the results and possibly provide a stronger correlation between the pKa of the modification and its inhibitory quality. Also due to time constraints, the assays were not run on the same day, which could have affected the results, due to changes in environment in the building where the assays were conducted. Further research can be conducted making modifications to the amino acids other than the first tyrosine in the parent compound. Advanced research can also be conducted using other Tendamistat based peptides, possibly involving the other important segments in the Tendamistat structure. Further experimentation can explore other potential α-amylase inhibitors including additional study of the ones previously mentioned and deriving others from various *Streptomyces* organisms.

Literature Cited

"3,5-Dibromotyrosine" ChemDB: The UC Irvine ChemDB. 25 Feb 2007. <http://cdb.ics.uci.edu/CHEM/Web/cgibin/ChemicalDetailWeb.py?chemical_id=4726513>.

"Alpha Amylase" The Medical Counsel: Laboratory for Molecular Biology. 25 Feb 2007. 2004. <http://www2.mrc-lmb.cam.ac.uk/>.

"Basic Steps in Solid Phase Peptide Synthesis Using Fmoc-Chemistry." Sigma-Aldrich. 2007. Sigma-Aldrich Company. 26 Mar. 2007 <http://www.sigmaaldrich.com/Brands/Sigma_Genosys/Custom_Peptides/Key_Resources/Solid_Phase_Synthesis.html>.

Cox, M. M., and Nelson, D. L. Principles of Biochemistry. 4th Ed. New York: W.H. Freemand and Company, 2005.

Dall'Antonia, F. "Research: Methodical Studies of Protein-B-Values." Structural Chemistry Department at the University of Göttingen. 25 Feb 2007. 26 Jun 2006. <http://shelx.uni-ac.gwdg.de/~fabio/endwkcon.htm>.

Heyl, D.L., Fernandes, S., Khullar, L., Stephens, J., Blaney, E., Opang-Owusu, H., Stahelin, B., Pasko, T., Jacobs, J., Bailey, D., Brown, D., and Milletti, M.C. (2005). "Correlation of LUMO Localization with the a-Amylase Inhibition Constant in a Tendamistat-Based Series of Linear and Cyclic Peptides." Bioorganic and Medicinal Chemistry, 13, 4262-4268.

Heyl, D.L., Schullery, S., Renganathan, K., Jayamaha, M., Rodgers, D., and Traynor, J. (2003) "pKa and Volume of Residue One Influence δ/α Opioid Binding: QSAR Analysis of Tyrosine Replacement in a Nonselective Deltorphin Analog" Bioorganic and Medicinal Chemistry, 11/17: 3761-3768.

Hirayama, K., Takahashi, R., Akashi, S., Fukuhara, K., Oouchi, N., Murai, A., Arai, M., Murao, S., Tanaka, K., and Nojima, I. (1987). "Primary Structue of Pain I, an α-Amylase Inhibitor from *Streptomyces corchorushii*, Determined by the Combination of Edman Degradation and Fast Atom Bombardment Mass Spectrometry." Biochemistry, 26: 6483-6488.

Hoffman, O., Vertesy, L., and Braunitzer, G. (1985). "The Primary Structure of α–Amylase Inhibitor Z-2685 from *Streptomyces parvullus* FH-1641. Sequence Homology Between Inhibitor and α-Amylase." Biological Chemistry Hoppe-Seyler, 366, 12: 1161-1168.

Katsuyama, K., Iwata, N., and Shimazu, A. (1992). "Purification and Primary Structure of Proteinous α-Amylase Inhibitor from *Streptomyces chartreuses*." Bioscience, Biotechnology, and Biochemistry, 56, 12: 1949-1954.

Lee, S., Gepts, P.L., and Whitaker, J.R. (2002). "Protein Structures of Common Bean (*Phaseolus vulgaris*) α-Amylase Inhibitors." Journal of Argiculture and Food Chemistry, 50: 6618-6627.

Machius, M., Vertesy, L., Huber, R., and Wiegand, G. (1996). "Carbohydrate and Protein-based Inhibitors of Porcine Pancreatic α-Amylase: Structure Analysis and Comparison of Their Binding Characteristics" Journal of Molecular Biology, 260: 409-421.

"Meta-Tyrosine" ChemicalLand21.com. 25 Feb 2007. 2000. <http://www.chemicalland21.com/lifescience/foco/m-TYROSINE.htm>.

Sefler, A.M., Kozlowski, M.C., Guo, T., and Bartlett, P.A. (1997). "Design, Synthesis, and Evaluation of a Depsipeptide Mimic of Tendamistat" Journal of Organic Chemistry, 62: 93-102.

Sumitani, J., Kawaguchi, T., Hattori, N., Murao, S., and Arai, M. (1993). "Molecular Cloning and Expression of Proteinaceous α-Amylase Inhibitor Gene from *Streptomyces nitrosporeus* in *Escherichia coli.*" Bioscience, Biotechnology, and Biochemistry, 57, 8: 1243-1248.

"Tendamistat." Protein NMR Structure Gallery. 13 Dec. 2005 <http://www-nmr.cabm.rutgers.edu/photogallery/structures/html/page17.html>.

Vertesy, L, V Oeding, R Bender, K Zepf, and G Nesemann. (1984). "Tendamistat (HOE 467), a Tight-Binding Alpha-Amylase Inhibitor from Streptomyces tendae 4158. Isolation, biochemical properties." European Journal of Biochemistry, 141: 505-512.

Vihinen, M. and Mantsala, P. (1989). "Microbial Amylolytic Enzymes." Critical Reviews in Biochemistry and Molecular Biology, 24: 329-418

Wiegand, G., Epp, O., and Huber, R. (1995). "The Crystal Structure of Porcine Pancreatic α-Amylase in Complex with the Microbial Inhibitor Tendamistat" Journal of Molecular Biology, 247: 99-110.

Yoshlda, M., Nakai, T., Fukuhara, K., Saitoh, S., Yoshikawa, W., Kobayashi, Y., and Nakamura, H. (1990). "Three-Dimensional Structure of an α-Amylase Inhibitor HAIM as Determined by Nuclear Magnetic Resonance Methods." Journal of Biochemistry, 108, 2: 158-165.